UNCERTAINTY QUANTIFICATION AND DESIGN UNDER UNCERTAINTY FOR METALLIC SYSTEMS

Sensitivity Assessment on Homogenized Stress–Strain Response of Ti-6Al-4V Alloy

MOHAMED ELLEITHY (1), 1,2 HENGDUO ZHAO, 1,3 and PINAR ACAR 1,4

1.—Department of Mechanical Engineering, Virginia Tech, Blacksburg, VA 24061, USA.
2.—e-mail: melleithy@vt.edu. 3.—e-mail: henryz@vt.edu. 4.—e-mail: pacar@vt.edu

The objective of this study is to investigate the effects of uncertainty of temperature and crystallographic orientations on the homogenized stress-strain response of Ti-6Al-4V alloy. The dual-phase Ti-6Al-4V alloy is an exceptional candidate for various applications in the aerospace field owing to its remarkable specific strength and significant mechanical properties at elevated temperatures. First, the hardening parameters are calibrated using a crystal plasticity finite element computational model. Once the crystal plasticity model parameters are calibrated by minimizing the error between experimental and predicted stress-strain curve behavior, the sensitivity of the predicted homogenized mechanical behavior to the temperature and crystallographic orientations is also analyzed. The findings of this work can be utilized to predict the alloy's homogenized mechanical properties, along with the characterization of the underlying microstructure at a specified temperature and orientation for a precise volume fraction of alpha and beta phases of the alloy. Furthermore, both the temperature and microstructural orientations are examined under a variation of 2% and 10%, respectively, to evaluate the uncertainty propagation on the mechanical response.

INTRODUCTION

The aerospace and biomedical industry heavily relies on metallic materials including Titanium-Aluminum alloys due to their exceptional mechanical properties such as high strength, low density, and excellent corrosion resistance across a diverse range of operating temperatures. ^{1–4} The microstructures of these alloys are the primary determinant of their unique performance and physical characteristics. ⁵ Ensuring the success of applications requires the crucial task of monitoring and predicting material properties under varying temperatures and orientations.

Titanium and its alloy can be categorized into five alloy families, namely α -Ti, near α alloys, $\alpha + \beta$, β -alloys, and intermetallic compounds based on Williams' "Titanium." Structural applications often require high-strength titanium alloys, which

typically consist of a two-phase $(\alpha + \beta)$ microstructure. This $\alpha + \beta$ phase configuration is widely utilized and finds extensive application in various industries. ^{7,8}

The mechanical performance of metallic materials can be explored under large deformations using the crystal plasticity finite element (CPFE) method. The CPFE method is a computational technique used to simulate and analyze the behavior of polycrystalline materials undergoing deformation. It combines the principles of crystal plasticity, which considers the plastic deformation mechanisms at the crystal level, with the finite element method, which discretizes the material into finite elements for numerical analysis.

In the field of materials science and engineering, the behavior of metallic alloys is often governed by complex microstructural interactions, and as a result, there is inherent uncertainty in their material properties. Uncertainty arises due to a variety of factors, such as variations in processing parameters, microstructural heterogeneity, temperature range of the operation and post-processing, etc. These factors can lead to variations in the material

properties, such as strength, ductility, and toughness, which can impact the performance of the material in different applications. ^{10,11}

Understanding and quantifying this uncertainty is crucial for predicting the performance of these materials under different conditions and ensuring their suitability for specific applications. 12 In addition, uncertainty quantification can also help guide the design and optimization of materials. ^{13,14} By identifying the sources of uncertainty, it is possible to develop more accurate and reliable models for predicting material properties and designing alloys with improved performance. The state-of-the-art utilizes computational methods to model microstructural uncertainty to estimate the variations in crystallographic texture, grain size distribution, and homogenized material properties including elasto-plastic stress-strain response. 15-20 Studies also include the identification of the uncertainty on the deformation behavior as a result of the microstructural uncertainty arising from thermomechanical processing²¹ and computation of the variations in elastic properties due to the uncertainty of microstructure geometry, single-crystal elastic constant values, and crystallographic texture. 22 We refer the readers to the summary study in Ref. 23 on the state-of-the-art uncertainty quantification algorithms applied to small-scale materials science problems. In this study, we model the variations related to the measurements for temperature and crystallographic texture and their propagation on the homogenized elasto-plastic stressstrain behavior of Ti-6Al-4V alloy. In particular, this study extends our group's preliminary work on the quantification and modeling of microstructural texture uncertainty on homogenized mechanical properties^{23–29} by modeling the effects of the uncertainty of both temperature and microstructural texture.

This study utilizes the CPFE method to investigate the deformation behavior of Ti-6Al-4V alloy. Initially, an optimization algorithm is employed to simulate and accurately match the stress and strain curves with experimental data. Subsequently, the impact of the uncertainty potentially arising from the measurements of temperature and crystallographic orientations on the material properties is thoroughly analyzed. This comprehensive examination provides valuable insights into the alloy's deformation behavior and the consequent impact of uncertainty on its performance.

COMPUTATIONAL FRAMEWORK

Crystal Plasticity Modeling

The implementation of a Crystal Plasticity Finite Element (CPFE) model is used to create an accurate multi-scale framework to investigate the elastic and plastic mechanical properties of the multi-phase Ti-6Al-4V alloy. A proprietary CPFE model accounts for the microscopic texture, grain orientation, active

phase-specific dislocation slip systems, and single-crystal values for the elastic stiffness tensor in addition to the slip hardening parameters to estimate Ti-6Al-4V's mechanical performance under complex, user-prescribed boundary conditions in a time-efficient manner. Within this study, Anand and Kothari's rate-independent, single-crystal constitutive model³⁰ is adopted to calibrate Ti-6Al-4V crystal plasticity hardening parameters at 21°C, which can consequently be used to predict the alloy's homogenized stress–strain behavior. The hardening moduli $(h^{\alpha\beta})$ used in the aforementioned constitutive model is represented by the following equation: $^{30-32}$

$$h^{lphaeta} = [q + (1-q)\delta^{lphaeta}]h^eta$$
 (no sum on eta) (1)

where $\delta^{\alpha\beta}$ represents the Kronecker delta function, q represents the latent hardening ratio, and h^β is the single-crystal slip hardening rate. The values 1.0 and 1.4 are generally used to describe the magnitude of the latent hardening ratio that matches a coplanar and non-coplanar slip system, respectively. The slip systems of the hexagonal close-packed (HCP) alpha-phase microstructure are assumed to be non-coplanar, while the simulation for the body-centered cubic (BCC) beta-phase microstructure assumes a coplanar slip system. The following expression for the single-crystal slip hardening rate is inclusive of the alloy's hardening parameters h_0 , s_s , and a:

$$h^{\beta} = h_0 \left(1 - \frac{s^{\beta}}{s_s} \right)^a \tag{2}$$

where h_0 is the hardening modulus, s_s is the saturation stress, s_β is the critical resolved shear stress, and a is the power law exponent. The slip systems considered in the realm of the calibration study are the basal < a >, prismatic < a >, pyramidal < a >, and pyramidal first < c + a > slip systems (Table I).

The formulation of the elastic stiffness tensor for the HCP crystalline structure, prior to CPFE deformation simulation, assumes a transversely isotropic condition that abides by the independence of five main constituents under the following conditions: $C_{11} = C_{22}, \ C_{12}, \ C_{13} = C_{23}, \ C_{33}, \ C_{55}, \ \text{and} \ C_{44} = (C_{11} - C_{12})/2$. Furthermore, Table II holds beta-phase elastic stiffness in three independent components corresponding to a BCC structure which fall under the following conditions: $C_{11} = C_{22} = C_{33}, \ C_{12} = C_{13} = C_{23}, \ \text{and}$

Table I. Ti-6Al-4V elastic stiffness tensor components for the alpha-phase at $21^{\circ}C^{34}$

C_{11}	C_{33}	C_{55}	C_{12}	C_{13}
164.7 GPa	82.5 GPa	61.8 GPa	175.2 GPa	48.5 GPa

2982 Elleithy, Zhao, and Acar

Table II. Ti-6Al-4V elastic stiffness tensor components for the beta-phase at $21^{\circ}C^{34}$

C_{11}	C_{55}	C_{12}	
104.6 GPa	148.9 GPa	71.3 GPa	

 $C_{44} = C_{55} = C_{66}$. The material-specific elastic stiffness tensor values for alpha and beta phases are calibrated at room temperature in Refs. 33–35.

Crystal Plasticity Model Calibration with Optimization

One of the primary objectives of the present work is to calibrate the crystal plasticity hardening parameters of Ti-6Al-4V alloy at a temperature of 21°C. This is achieved through the integrated use of the CPFE model and an interior-point-convex optimization technique. Calibration is required due to the lack of analytical or experimental quantification of the hardening parameters associated with the constitutive model implemented in this study. The employment of an interior-point optimization technique is favorable for its leverage with respect to a largely scaled problem that engages several active variables, as well as the successive comparison between discretized data points, similar to the work presented. 36 The algorithm is capable of allocating a minimum between the upper and lower bounds via the convergence of the objective function in a robust and efficient manner, thus allowing for a relatively low computational time and distinctive numerical stability in accordance with a high-fidelity CPFE model.

In order to find the optimum set of values corresponding to the initial slip resistances (s_0) , hardening moduli (h_0) , saturation stress (s_s) , and power law exponent (a) within the room temperature range, experimentally measured stress-strain data under simple compression are referenced within the optimization algorithm. The objective function aims to minimize the sum of the squared relative error percentages between the predictions of the CPFE simulation and the experimental data. Establishing the sum of squared errors (SSE) as an objective function is necessary to account for the difference in the order of magnitude between the stress-strain curve parameters used in the objective function generation. The optimization problem formulation is characterized by the following equation:

$$minimize SSE(s_0, h_0, s_s, a)$$
 (3)

$$\begin{aligned} \text{SSE} &= \left(\frac{E^{\text{pred}} - E^{\text{exp}}}{E^{\text{exp}}}\right)^2 + \left(\frac{\sigma_y^{\text{pred}} - \sigma_y^{\text{exp}}}{\sigma_y^{\text{exp}}}\right)^2 \\ &+ \sum_{i=1}^4 \left(\frac{b_i^{\text{pred}} - b_i^{\text{exp}}}{b_i^{\text{exp}}}\right)^2 \end{aligned} \tag{4}$$

where its components are designated in terms of the elastic stiffness moduli (E), yield strength (σ_y) , and four successive slope increments $(b_i$ where i=1,2,3,4) along the plastic region extracted from the stress–strain curve. The superscripts exp and pred denote experimental and predicted data, respectively. These quantifying parameters are illustrated in Fig. 1.

The algorithm is set to obtain a total of 10 design variables pertaining to crystal plasticity hardening parameters at 21°C. The initial slip resistance values, along with the hardening moduli are established as variables particular to basal $\langle a \rangle$, prismatic $\langle a \rangle$, pyramidal $\langle a \rangle$, pyramidal $\langle c + a \rangle$ slip systems, while the saturation stresses and power law exponent are assumed to represent an individual variable for the HCP characteristic slipsystems defined. The beta-phase hardening parameters are not included as independent variables in the calibration process for the lack of quantitative bounds that may be set for the BCC slip systems; henceforth the values are taken to be equivalent to those of alpha-phase basal $\langle a \rangle$, prismatic $\langle a \rangle$, and pyramidal $\langle c + a \rangle$, which is based on an extension of Ozturk's assumption in Ref. 35.

Uncertainty Quantification (UQ) for Temperature and Crystallographic Orientation

Uncertainty Quantification for Temperature

Upon the calibration of the crystal plasticity parameters at a nominal temperature of 21°C, an uncertainty quantification (UQ) approach is applied to observe the sensitivity and variations of the elastic and plastic stress-strain curve parameters as a response to distinctive changes with respect to temperature and initial crystallographic orientations. The UQ for temperature is carried out by assuming $\pm 2\%$ variations around the expected value using a Gaussian distribution representation, while the initial crystallographic orientation described by a Rodrigues space vector is assumed to remain constant. The examination of the proposed minuscule change in temperature, which emulates possible discrepancies in temperature measuring devices, will help assess the reliability of the CPFE model's predictions.

In an effort to represent the appropriate changes to the CPFE input parameters that are susceptible to change according to thermal variation, the slip directions and plane-normal values are mitigated as a consequence of the c/a ratio change with temperature in alpha-phase.³⁷ Moreover, the elastic properties at the prescribed temperature represent baseline values to the linearly decreasing change of stiffness components with respect to temperature, which is documented as a unique set of slopes by Ghosh and Ozturk.^{34,35} Furthermore, the initial slip resistance parameters for each slip system in the

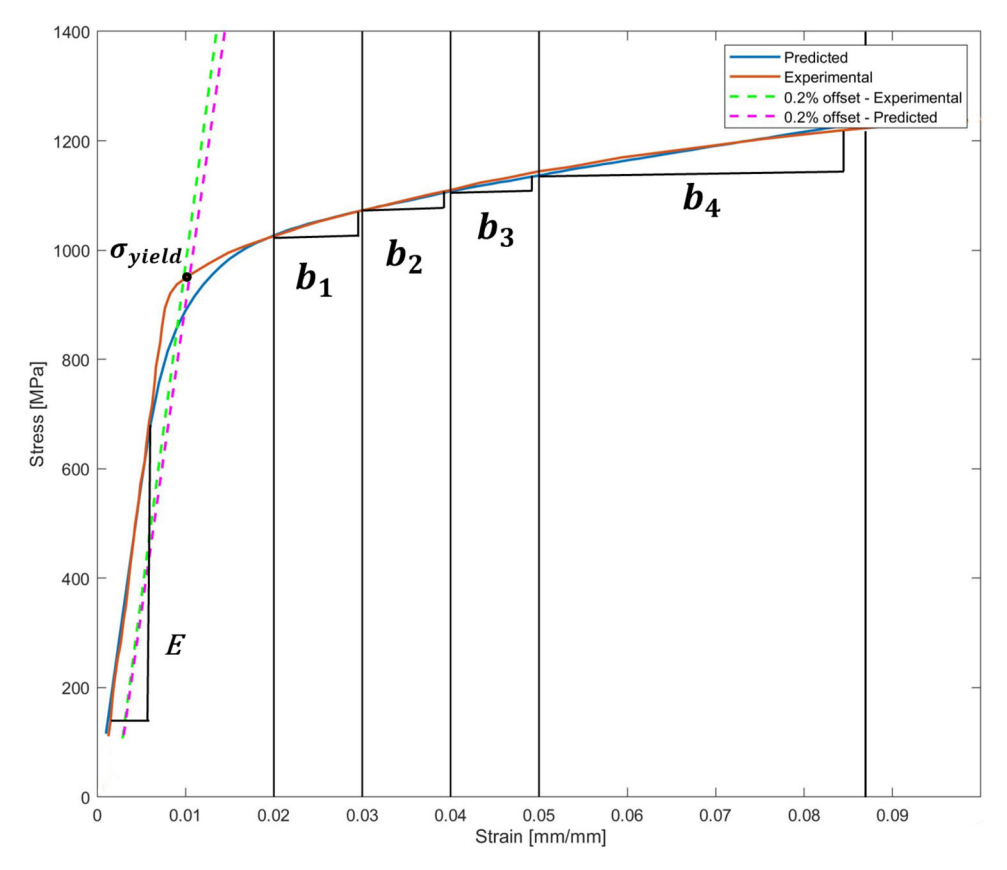


Fig. 1. Experimental and CPFE-predicted stress-strain curves for Ti-6Al-4V at room temperature.

HCP configuration are adjusted according to the temperature change via the application of the following equation: 34,35

$$s^{\alpha} = s_{\mathrm{ref}}^{\alpha} \left(\frac{T}{T_{\mathrm{ref}}} \right)^{p}$$
 (5)

where $T_{\rm ref}$ is taken to be equivalent to 21°C, $s_{\rm ref}$ is the initial slip resistance value at 21°C, and p is approximated to a value of $-1.^{34,35}$ However, the hardening moduli, saturation stress, and power law exponent remain constant throughout the sensitivity analysis due to the lack of literature on the crystal plasticity constitutive model parameters as a function of thermal variation, which would require an adequately representative experimental procedure for characterization purposes of high cost.

Uncertainty Quantification for Crystallographic Orientation

The mechanical properties of $\alpha + \beta$ Titanium alloys are intimately connected to the characteristics of their microstructures. The development of a predictive model for material properties based on orientation changes requires a substantial and comprehensive database. The original set of experimental orientations serves as the baseline data set for simulating stress–strain curves in the CPFE model. Moreover, Young's modulus and yield strength are derived from

these curves and utilized for comparative purposes with data from varied orientations, alongside the evaluation of uncertainty. Variations in process parameters result in corresponding changes to the orientation values. To simulate the effect of microstructural changes due to variations microstructure orientation, a random perturbation of $\pm 10\%$ is introduced to the orientation values using the MCS method, while maintaining a constant temperature of 21°C. Additional 1000 simulations are then performed to supplement the limited experimental data. Because the properties are dependent on microstructure, the additional simulation would suggest how they are related. These perturbed orientations serve as input parameters for the CPFE model, which calculates the corresponding strain-stress curve. Furthermore, the uncertainty propagation on mechanical properties, including the yield strength and Young's modulus, is computed. The percentage error between the baseline data set and experiential data is analyzed to evaluate the propagation of uncertainty throughout the CPFE model.

RESULTS AND DISCUSSIONS

Calibration Results for Crystal Plasticity Model Parameters

The computational framework integrating the rate-independent CPFE model, and the interior-

Elleithy, Zhao, and Acar

point optimization algorithm identify the crystal plasticity parameters shown in Table III. In consistency with the quantified elastic and plastic variables defined through Fig. 1 mentioned a priori, the model attains a local minimum to the objective function devised with candidate parameters within the user-defined minimum and maximum ranges of the crystal plasticity variables of interest. Moreover, the set of alloy-specific parameters results in the homogenized stress-strain curve, illustrated in Fig. 2, along with the experimental curve. Consequent to the nullified objective function achieved through the optimization process, the misalignment that is visually noted in Fig. 2 is attributed to the parameters' ranges along the stress-strain curve, which can be mitigated through the attribution of additional variables within the problem formulation; however, such action introduces a costly increment to the solution and is not yet theorized to evaluate design variables of interest within a feasible region. The validation of the alloy's hardening parameters provides a baseline or reference for the projection of the stress-strain behavior as a result of the slip-system-specific initial slip resistance values. Additionally, the calibrated set of candidate parameters provides a preliminary basis for the prediction of the viscoelastic and viscoplastic behavior of the alloy, which may be exploited for computation purposes that may, in turn, decrease the material experimentation costs. Furthermore, acquiring the set of Ti-6Al-4V's candid plasticity parameters may be extended for metallic alloys' design objectives that could be carried out via Computer-Aided Design (CAD) and Finite Elements Method (FEM) methods that are able to simulate contemporary additive manufacturing mechanisms, thus improving the overall approach to multi-scale structural hierarchy design components fabricated from Ti-6Al-4V.

Uncertainty Propagation on Elasto-Plastic Stress-Strain Behavior due to Variations of Temperature

Post-calibration of Ti-6Al-4V model-specific crystal plasticity parameters, a Gaussian distribution within a $\pm 2\%$ range, using 1000 samples with the MCS method, about the mean temperature of 21°C is generated to investigate the model's sensitivity to thermal changes. Figure 3 demonstrates that the

2% variation in temperature leads to insignificant changes in the elastic stiffness and yield strength. This is further supported by the histogram plots for Young's modulus and yield strength in Fig. 4 demonstrating the uncertainty propagation in these parameters. The elastic parameters measured corresponding to the temperature values tested via the CPFE model are found to be inversely proportional to the changes in temperature as agreed by the analytical relationship between the stiffness tensor constituents and temperature.

Such direct proportionality cannot be generalized to the remaining parameters describing the plastic deformation region. That is due to the assumption of the hardening moduli, saturation stresses, and power law exponent values as constants, as well as the absence of a deterministic relationship between the plastic region slopes and temperature. The change in the slopes is noted to be following a close-to-normal distribution as a response to the Gaussian input for the temperature values within the specified bounds. However, Fig. 5a and c illustrate a right-handed skewed and left-handed enumeration of the first and third slope values respectively, which may suggest a non-linear correlation between the slopes and the thermal variations. Furthermore, the absolute error percentages between the CPFE model and experimental data for the plastic region are illustrative of the thermal effect on the alloy's mechanical behavior. The maximum absolute error percentages recorded for the plastic region slopes are as follows: $b_1 \approx 4.1\%$, $b_2 \approx 10.5\%$, $b_3 \approx 23.9\%$, and $b_4 \approx 7.6\%$. Accordingly, the effects of the thermal variations on the elastic stiffness, HCP slip systems definition, and slip resistances provide an insight into the potentially quantifiable correlation between Ti-6Al-4V's hardening behavior and temperature that is accompanied by the comprehension of the model's temperature's sensitivity within a viable extent of uncertainty.

Uncertainty Propagation on Elasto-Plastic Stress-Strain Behavior due to Variations of Initial Texture

To investigate the effects of the microstructural texture uncertainty on the stress-stress behavior, a post-calibration procedure is conducted on the model-specific crystal plasticity parameters. This involves generating 1000 samples representing

Table III. Ti-6Al-4V (alpha-phase) calibrated crystal plasticity parameters at 21° C and strain-rate of $0.01 \, s^{-1}$

Slip system	s_0	h_0	s_s	a
Basal $\langle a \rangle$	388.3 MPa	641.6 MPa	724.1 MPa	1.8
Prismatic $\langle a \rangle$	383.7 MPa	509.9 MPa	724.1 MPa	1.8
Pyramidal <a>	686.3 MPa	610.2 MPa	724.1 MPa	1.8
Pyramidal $\langle c + a \rangle$	423.8 MPa	642.1 MPa	724.1 MPa	1.8

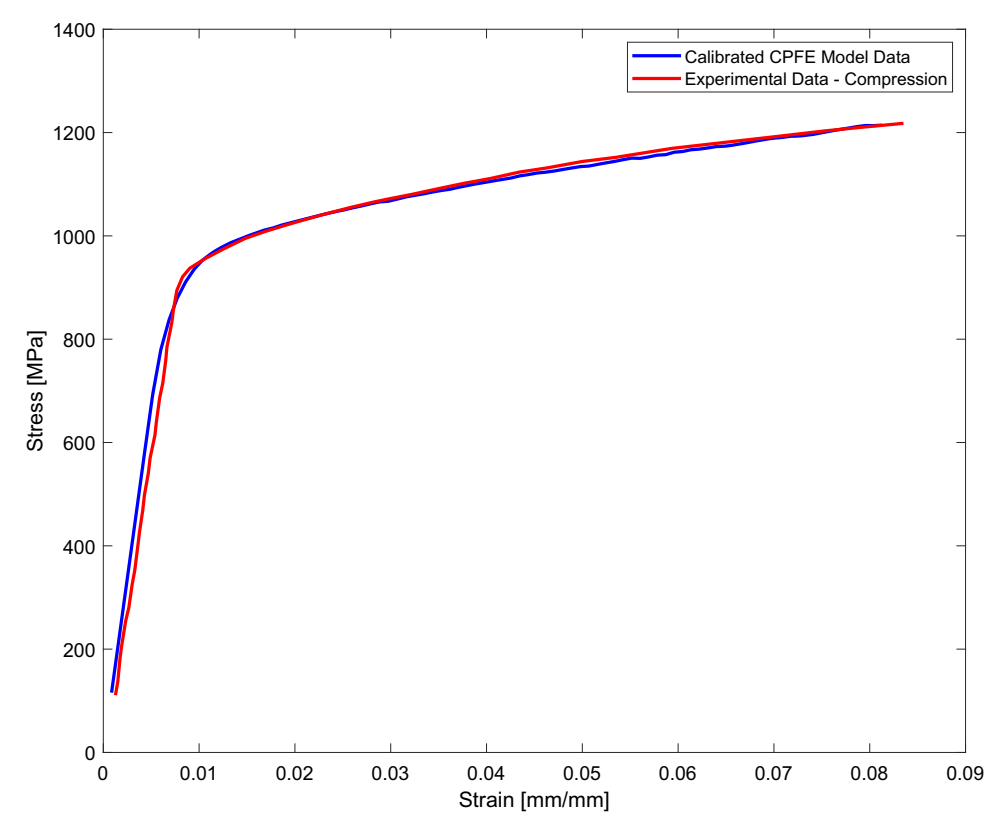


Fig. 2. CPFE-predicted stress-strain curve for calibrated parameters in comparison to experimental data at 21°C.

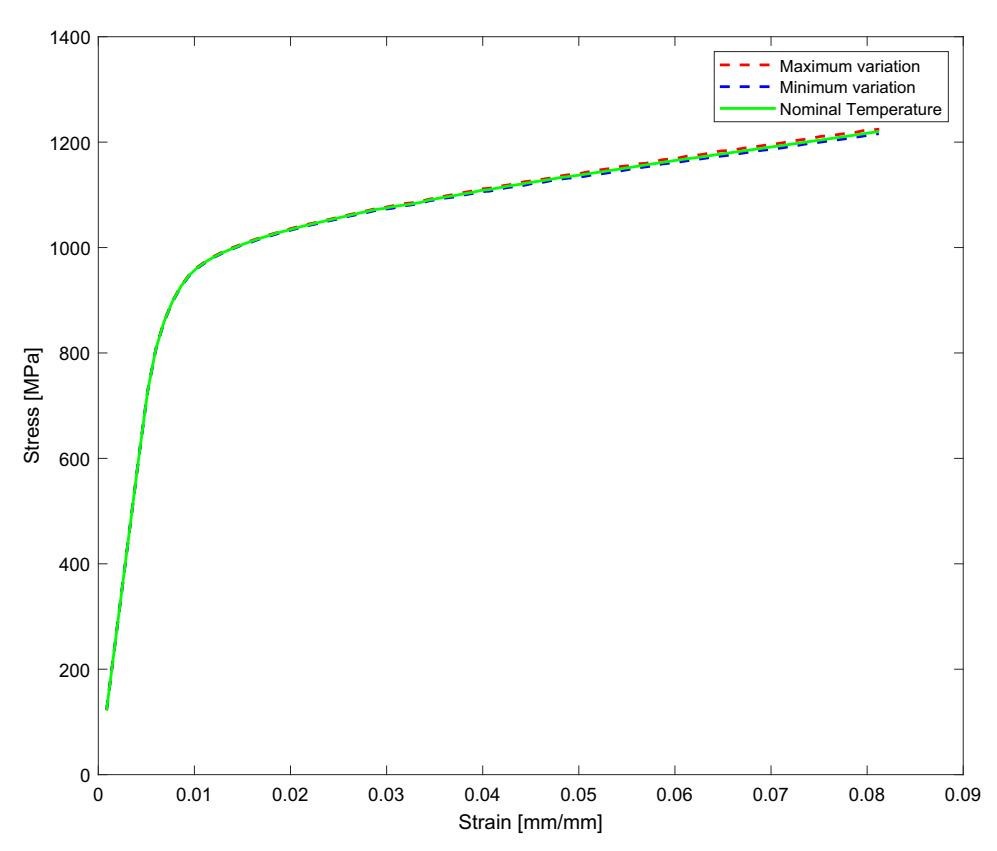


Fig. 3. Stress-strain curves corresponding to the maximum and minimum variations as a result of the uncertainty of temperature in comparison to the nominal data.

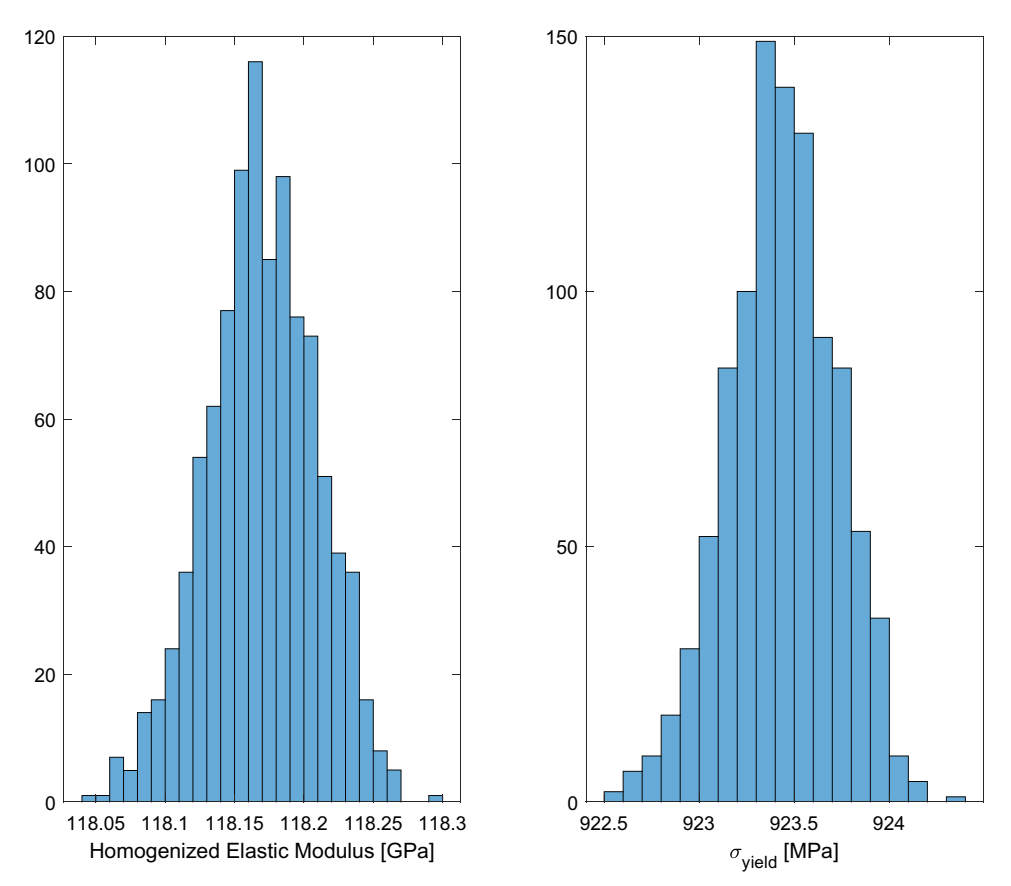


Fig. 4. Frequency histograms for the computed Ti-6Al-4V elastic parameters as a result of 2% variation over nominal room temperature.

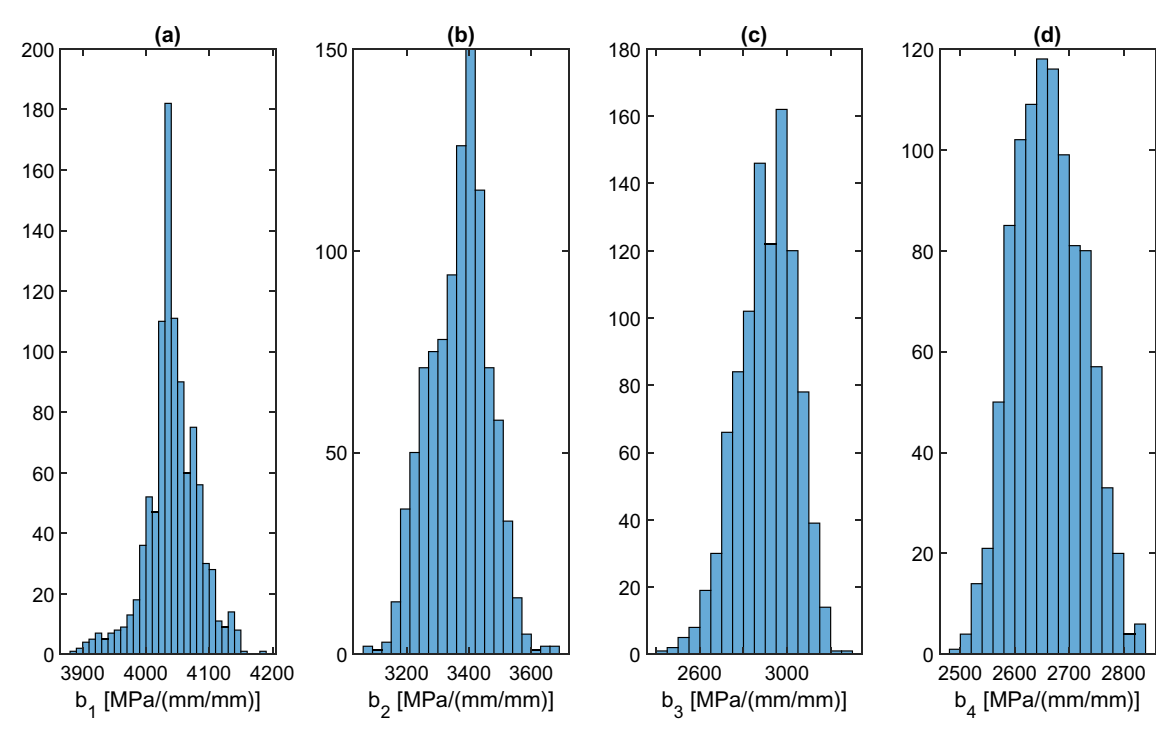


Fig. 5. Frequency histograms for the computed Ti-6Al-4V plastic parameters as a result of 2% variation over nominal room temperature.

deviations from the original initial texture data by applying a Gaussian distribution assumption within a $\pm\,10\%$ range by following the findings of Acar and Sundararaghavan^{24,25} on the variations of microstructural texture. The objective is to evaluate the model's response to orientation changes in crystallographic orientations, particularly concerning the crystal plasticity parameters mentioned earlier.

The stress-strain relationship for the nominal orientation, along with the maximum and minimum variations observed during the simulation, is depicted in Fig. 6. The nominal data indicates a

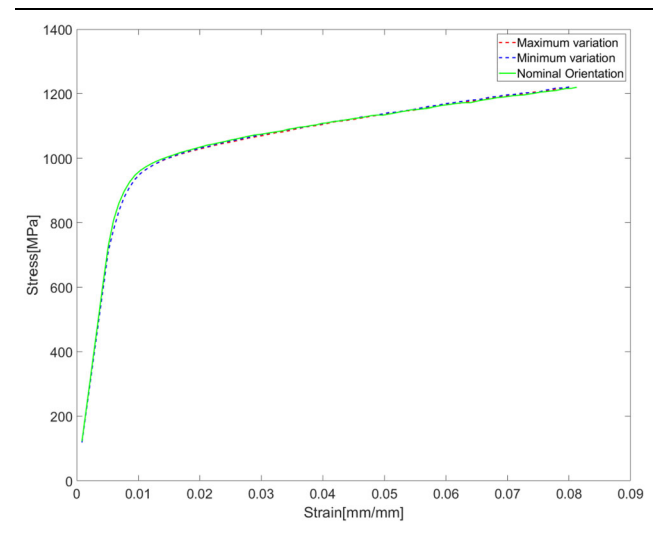


Fig. 6. Stress-strain curves corresponding to the maximum and minimum variations as a result of the uncertainty of crystallographic orientations in comparison to the nominal data.

yield strength of 908.46 MPa and Young's modulus of 115.09 GPa. Throughout the simulation, the yield strength exhibits a maximum value of 909.59 MPa and a minimum value of 907.67 MPa, while the corresponding range for Young's modulus is 115.24-114.94 GPa. The maximum absolute percentage error is 0.12% for the yield strength and 0.26% for Young's modulus. The result demonstrates minimal deviation within the 10% range of orientation changes. Histogram plots in Fig. 7 present the distributions of the elastic modulus and yield strength obtained from the 1000 simulations using the MCS method. Both diagrams display a slightly right-skewed distribution, suggesting no direct correlation between the material properties and the orientation subjected to changes according to the Gaussian distribution. This indicates that the variation in material properties is not linearly dependent on changes in the orientation within the specified ranges. Figure 8 illustrates the distributions of the slopes within the plastic region in response to the corresponding orientation changes. It is observed that slopes b_1 and b_4 exhibit a rightskewed distribution, while slopes b_2 and b_3 display a left-skewed distribution. The maximum absolute percentage error for the slopes of the plastic region for b_1 , b_2 , b_3 , and b_4 are 9.90%, 15.8%, 14.5%, and 12.9%, respectively. This finding suggests that there is no direct correlation between the slope within the plastic region and the orientation changes. The absence of a consistent relationship implies that changes in orientation do not exert a deterministic influence on the slope characteristics within the plastic region.

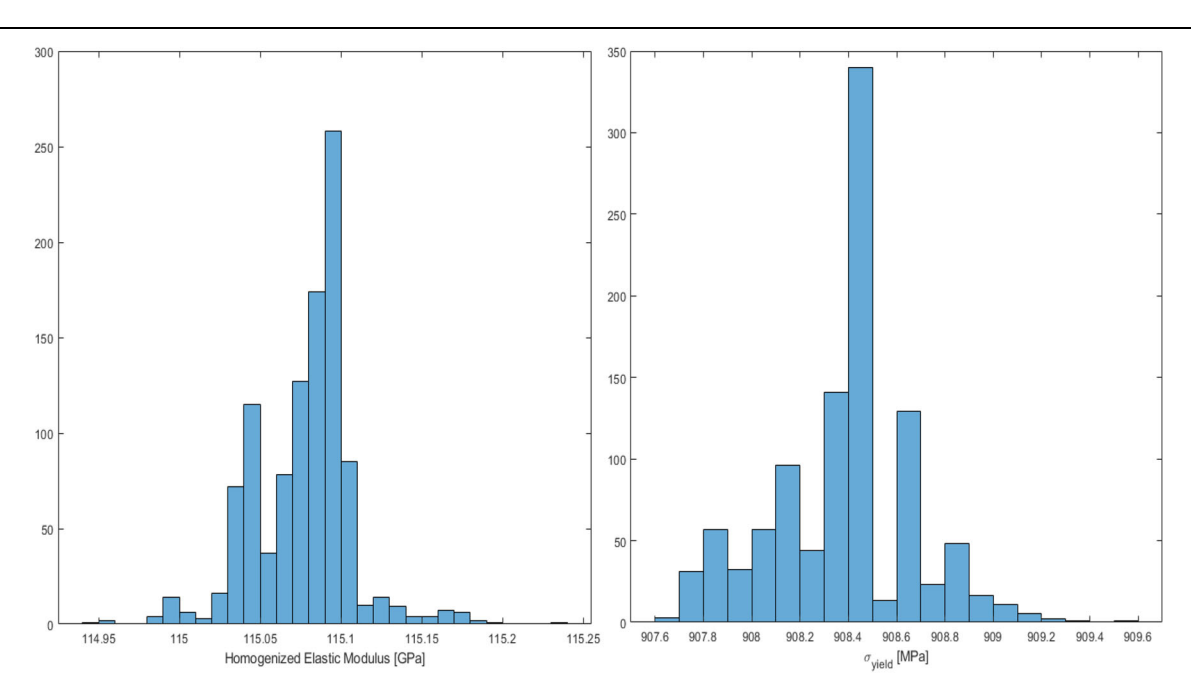


Fig. 7. Frequency histograms for elastic modulus and yield strength obtained using 1000 samples representing 10% variation over microstructural orientations with MCS method.

2988 Elleithy, Zhao, and Acar

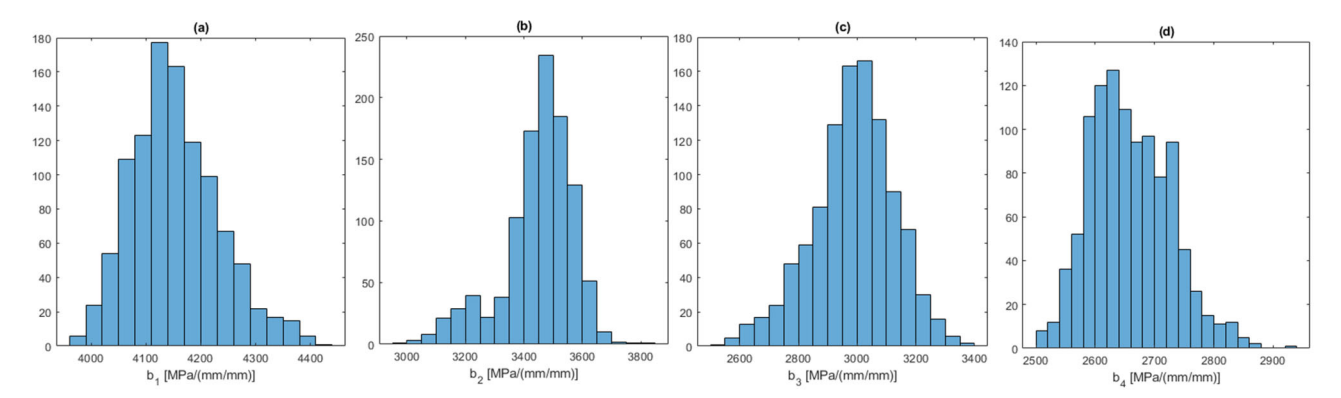


Fig. 8. Frequency histograms for plastic region slopes obtained using 1000 samples representing 10% variation over microstructural orientations with MCS method.

In summary, the analysis reveals minimal deviation in the stress-strain relationship across a range of orientation changes. Material properties, such as elastic modulus and yield strength, do not show a direct correlation with orientation variations. Moreover, the slope characteristics within the plastic region are not consistently affected by changes in orientation.

CONCLUSION

This study investigates the effects of uncertainty on the homogenized stress-strain behavior of Ti-6Al-4V alloy. It starts with the calibration of the crystal plasticity parameters, signifying a computational understanding of the alloy's behavior at the specified temperature. In the calibration study, the optimization process proves its substantiality in the determination of plausible crystal plasticity parameters that are influenced by the subjective case of the specimen's manufacturing method that is relevant to the alloy's texture and overall mechanical capabilities under certain conditions. Next, deviations from the nominal temperature and crystallographic orientations are modeled to find the corresponding variations of the stress-strain response using the Monte Carlo Sampling (MCS) method. The findings for temperature variation demonstrate a non-linear connection between the alloy's plastic behavior and temperature while showing negligent influence over homogenized elastic modulus and yield strength. Moreover, the stress-strain relationship exhibits minimal deviation when subjected to variations in crystallographic orientations. The investigation further reveals that mechanical properties, including elastic modulus and yield strength, are not linearly correlated with changes in orientations. Additionally, the slope characteristics with the plastic region do not exhibit consistent effects in response to orientation variations. Future work may extend this study by investigating the effects of microstructural uncertainty in addition to the uncertainty of external

physical drivers (e.g., temperature) on the multiscale mechanical behavior ranging from micro-scale to component-scale.

ACKNOWLEDGEMENTS

The authors acknowledge financial support from the NSF CMMI Award #2053840 and the Young Faculty Award program by the Institute for Critical Technology and Applied Science (ICTAS) at Virginia Tech. We also thank Prof. John Allison from the Materials Science and Engineering Department at the University of Michigan and the Commonwealth Center for Advanced Manufacturing (CCAM) for the experimental data of Ti-Al alloys.

CONFLICT OF INTEREST

On behalf of all authors, the corresponding author states that there is no conflict of interest.

REFERENCES

- R.R. Boyer, Adv. Perform. Mater. 2, 349 https://doi.org/10. 1007/BF00705316 (1995).
- A.M. Khorasani, M. Goldberg, E.H. Doeven, and G.J. Littlefair, Biomater. Tissue Eng. 5, 593 https://doi.org/10.1166/jbt.2015.1361 (2015).
- W.D. Brewer, R.K. Bird, and T.A. Wallace, Mater. Sci. Eng. A 243, 299 https://doi.org/10.1016/S0921-5093(97)00818-6 (1998).
- C. Veiga, J.P. Davim, and A.J.R. Loureiro, Rev. Adv. Mater. Sci. 32(2), 133 (2012).
- G. Lütjering, Mater. Sci. Eng. A 243, 32 https://doi.org/10. 1016/S0921-5093(97)00778-8 (1998).
- J.C. Williams and R.R. Boyer, Metals 10(6), 705 https://doi. org/10.3390/met10060705 (2020).
- H.J. Rack and J.I. Qazi, Mater. Sci. Eng. C 26(8), 1269 h ttps://doi.org/10.1016/j.msec.2005.08.032 (2006).
- M. Peters, J. Kumpfert, C.H. Ward, and C. Leyens, Adv. Eng. Mater. 5(6), 419 https://doi.org/10.1002/adem.2003100 95 (2003).
- F. Roters, P. Eisenlohr, T.R. Bieler, and D. Raabe, Crystal Plasticity Finite Element Methods: In Materials Science and Engineering (John Wiley & Sons, Weinheim, 2010), pp44–
- A.K. Singla, M. Banerjee, A. Sharma, J. Singh, A. Bansal, M.K. Gupta, N. Khanna, A.S. Shahi, and D.K. Goyal, J. Manuf. Process. 64, 161 https://doi.org/10.1016/j.jmapro.20 21.01.009 (2021).

- L. Bian, S.M. Thompson, and N. Shamsaei, JOM 67, 629 h ttps://doi.org/10.1007/s11837-015-1308-9 (2015).
- P. Li, D.H. Warner, A. Fatemi, and N. Phan, Int. J. Fatigue 85, 130 https://doi.org/10.1016/j.ijfatigue.2015.12.003 (2016).
- 13. G.T. Loughnane, A Framework for Uncertainty Quantification in Microstructural Characterization with Application to Additive Manufacturing of Ti-6Al-4V (Wright State University, 2015). https://corescholar.libraries.wright.edu/cgi/viewcontent.cgi?article=2732 &context=etd_all. Accessed 4 Apr 2023.
- S. Mahadevan, P. Nath, and Z. Hu, ASCE ASME J. Risk Uncertain. Eng. Syst. Part B Mech. Eng. 8(1), 010801 https://doi.org/10.1115/1.4053184 (2022).
- A. Chernatynskiy, S.R. Phillpot, and R. LeSar, *Ann. Rev. Mater. Res.* 43, 157 https://doi.org/10.1146/annurev-matsci-071312-121708 (2013).
- A. Creuziger, K. Syed, and T. Gnäupel-Herold, Scr. Mater.
 55 https://doi.org/10.1016/j.scriptamat.2013.10.017 (2014).
- 17. J. Luan, G. Liu, H. Wang, and A. Ullah, *J. Microsc.* 244, 214 https://doi.org/10.1111/j.1365-2818.2011.03531.x (2011).
- B. Hiriyur, H. Waisman, and G. Deodatis, Int. J. Numer. Methods Eng. 88(3), 257 https://doi.org/10.1002/nme.3174 (2011).
- L. Huyse, and M.A. Maes, J. Eng. Mech. 127(1), 27 https://doi.org/10.1061/(ASCE)0733-9399(2001)127:1(27) (2001).
- S. Sakata, F. Ashida, T. Kojima, and M. Zako, *Int. J. Solids Struct.* 45(3–4), 894 https://doi.org/10.1016/j.ijsolstr.2007.0 9.008 (2008).
- B. Kouchmeshky and N. Zabaras, Comput. Mater. Sci. 47(2), 342 https://doi.org/10.1016/j.commatsci.2009.08.010 (2009).
- P.J. Madrid, D. Sulsky, and R.A. Lebensohn, J. Microelectromech. Syst. 23(2), 380 https://doi.org/10.1109/JMEMS.2013.2279500 (2013).
- P. Acar, Prog. Mater. Sci. 117, 100723 https://doi.org/10.10 16/j.pmatsci.2020.100723 (2021).
- P. Acar, and V. Sundararaghavan, Acta Mater. 124, 100 h ttps://doi.org/10.1016/j.actamat.2016.10.070 (2017).
- P. Acar, and V. Sundararaghavan, AIAA J. 55(8), 2824 h ttps://doi.org/10.2514/1.J055689 (2017).
- P. Acar, Materials 12(11), 1773 https://doi.org/10.3390/ma 12111773 (2019).

- P. Acar, AIAA J. 58(8), 3569 https://doi.org/10.2514/1.J059 233 (2020).
- M. Hasan and P. Acar, AIAA J. 60(1), 461 https://doi.org/10. 2514/1.J060372 (2022).
- A. Senthilnathan and P. Acar, AIAA J. 60(8), 4969 https://doi.org/10.2514/1.J061455 (2022).
- L. Anand, and M. Kothari, J. Mech. Phys. Solids 44, 525 h ttps://doi.org/10.1016/0022-5096(96)00001-4 (1996).
- P. Acar, A. Ramazani, and V. Sundararaghavan, *Metals* 7, 459 https://doi.org/10.3390/met7110459 (2017).
- P. Acar, Integr. Mater. Manuf. Innov. 7(4), 186 https://doi. org/10.1007/s40192-018-0120-0 (2018).
- D. Deka, D.S. Joseph, S. Ghosh, and M.J. Mills, Metall. Mater. Trans. A 37, 1371 https://doi.org/10.1007/s11661-006-0082-2 (2006).
- 34. S. Ghosh, Final report: Multi-scale analysis of deformation and failure in polycrystalline titanium alloys under high strain-rates (Defense Technical Information Center, 2015). https://apps.dtic.mil/sti/pdfs/AD1007179. Accessed 6 Apr 2023.
- D. Ozturk, A. Shahba, and S. Ghosh, Fatigue Fract. Eng. Mater. Struct. 39, 752 https://doi.org/10.1111/ffe.12410 (2016)
- R. Zhou, K.H. Pang, A. Bisht, A. Roy, S. Suwas, and V.V. Silberschmidt, *Philos. Trans. A Math. Phys. Eng. Sci.* 378, 2162 https://doi.org/10.1098/rsta.2019.0105 (2020).
- F.R. Kaschel, R.K. Vijayaraghavan, A. Shmeliov, E.K. McCarthy, M. Canavan, P.J. McNally, D.P. Dowling, V. Nicolosi, and M. Celikin, *Acta Mater*. 188, 720 https://doi.org/10.1016/j.actamat.2020.02.056 (2020).

Publisher's Note Springer Nature remains neutral with regard to jurisdictional claims in published maps and institutional affiliations.

Springer Nature or its licensor (e.g. a society or other partner) holds exclusive rights to this article under a publishing agreement with the author(s) or other rightsholder(s); author self-archiving of the accepted manuscript version of this article is solely governed by the terms of such publishing agreement and applicable law.